Sensors operating at exceptional points: General theory

Jan Wiersig*
Institut für Theoretische Physik, Otto-von-Guericke-Universität Magdeburg, Postfach 4120, D-39016 Magdeburg, Germany
(Received 8 January 2016; published 4 March 2016)

A general theory of sensors based on the detection of splittings of resonant frequencies or energy levels operating at so-called exceptional points is presented. Exploiting the complex-square-root topology near such non-Hermitian degeneracies has a great potential for enhanced sensitivity. Passive and active systems are discussed. The theory is specified for whispering-gallery microcavity sensors for particle detection. As example, a microdisk with two holes is studied numerically. The theory and numerical simulations demonstrate a sevenfold enhancement of the sensitivity.

DOI: 10.1103/PhysRevA.93.033809

I. INTRODUCTION

Several modern sensor devices are based on the detection of frequency (energy-level) splittings. Examples are weak magnetic field sensors [1], nanomechanical mass sensors [2], bending curvature sensors [3], optical gyroscopes [4,5], microcavity sensors for single- or few-particle detection [6–8]. The basic principle is that the target signal is a perturbation which acts on a twofold-degenerate system representing the sensor. The perturbation then lifts the degeneracy resulting in a frequency or energy-level splitting which can be detected and quantified. All existing devices use a conventional degeneracy at which the energy levels degenerate but the eigenstates can always be chosen to be orthogonal to each other. As well known from quantum mechanical perturbation theory, a perturbation of strength ε acting on such a degeneracy leads to energy shifts and splitting proportional to ε. When ε and a second parameter are varied, the surfaces representing the energy levels form a double cone resembling a diabolo, a juggling toy. The degeneracy sitting at the apex of the cones is therefore called diabolic point (DP) [9].

However, DPs are not the only possible degeneracies in physical systems. In open wave/quantum systems there is another type of degeneracy called exceptional point (EP). At such a non-Hermitian degeneracy, not only eigenvalues but also the corresponding eigenstates coalesce [10–13]. Most of the studies, and also this paper, focus on EPs of order two, where exactly two eigenstates coalesce. Varying two parameters around such an EP reveals a complex-square-root topology of the surfaces representing the energy levels. A number of experiments have undoubtedly proven the existence of EPs in physical systems, e.g., in microwave cavities [14–16], in optical microcavities [17,18], in coupled atom-cavity systems [19], and in nonuniformly pumped lasers [20]. Furthermore, theoretical investigations reveal that EPs also appear in other systems, such as hydrogen atoms in crossed magnetic and electric fields [21] and photonic lattices [22,23]. If an EP of order two is subjected to a perturbation of strength ε, then the resulting energy splitting is generically proportional to $\sqrt{\varepsilon}$ [10,24]. The latter fact is consistent with the above-mentioned complex-square-root topology, having in mind that the parameter variation can be considered as a perturbation of the system at the EP.

In Ref. [25], it has been suggested to exploit this square-root dependence for sensing. The idea is that for sufficiently small perturbation, i.e., small ε, the frequency splitting of order $\sqrt{\varepsilon}$ at a EP is larger than the splitting of order ε at a DP. That means the sensitivity is enhanced at an EP if compared to a DP even though exactly the same perturbation is applied. The theory presented in Ref. [25] is restricted to a whispering-gallery (WG) microcavity sensor for particle detection. It is based on the validity of a two-state model with fixed azimuthal mode number. Numerical simulations on this system have demonstrated a 3.5-fold enhancement of the sensitivity. Meanwhile, this mechanism has been discussed in the context of parity-time (PT-) -symmetric coupled disk [26] and coupled nanobeam cavities [27]. Note that recently a similar square-root behavior at a Hopf bifurcation has been exploited in an optoelectromechanical sensor mimicking hair cells [28]. A rather different approach for microcavity sensors uses the sensitivity of the far-field pattern of emitted light near an EP [29].

The purpose of this article is to present a general theory of EP sensors for frequency-splitting detection. We prove that in general gain is needed for a straightforward experimental detection of the splitting. In the case of WG microcavity sensors the theory does not require the validity of the two-state model with fixed azimuthal mode number. We introduce a microcavity-sensor geometry and present numerical simulations that clearly show that for this system the two-state model with fixed azimuthal mode number is not a good approximation.

This paper is organized as follows. Section II derives the general theory. In Sec. III, the two-state model with fixed azimuthal mode number for microcavity sensors is reviewed. In Sec. IV, we present numerical results and compare the two different theoretical approaches. Section V contains a discussion. Some details of the theory are outsourced to the Appendix.

II. GENERAL THEORY

A. Exceptional point vs diabolic point

In this section, we present the general theory of sensors based on frequency- or energy-level-splitting detection operating at EPs. The existence of an EP requires the system to be non-Hermitian. The non-Hermiticity can originate from loss or gain in the material or through the boundaries of the system. For instance, the optical modes (the optical analog

*Corresponding author: jan.wiersig@ovgu.de

of energy eigenstates) in microcavities are subjected to losses due to absorption in the material and radiation to the exterior. As consequence, each mode has a finite lifetime and a finite spectral linewidth at its resonant frequency. These features can often be well described, at least locally, by a non-Hermitian effective Hamiltonian H (see, e.g., [30–37]). The dynamics of the state vector ψ is then governed by a Schrödinger-type equation ($\hbar$ is set to 1)

$$i\frac{d}{dt}\psi = H\psi. \tag{1}$$

For optical systems, such an equation of motion can be justified in the slowly varying envelope approximation in the time domain [38].

We assume that the sensor is a twofold-degenerate system which is described by a 2×2 Hamiltonian H_0. In the case of a DP, the matrix H_0 can be diagonalized, i.e., in its eigenbasis H_0 can be written as

$$H_0|_{\mathrm{DP}} = \begin{pmatrix} E_0 & 0 \\ 0 & E_0 \end{pmatrix}, \tag{2}$$

with complex eigenvalue E_0. At an EP, H_0 cannot be diagonalized but it can be transformed into the form

$$H_0|_{\mathrm{EP}} = \begin{pmatrix} E_0 & A_0 \\ 0 & E_0 \end{pmatrix}, \tag{3}$$

with complex eigenvalue E_0 and off-diagonal element $A_0 \neq 0$. By scaling the whole matrix we could replace A_0 by 1, which would result in the Jordan normal form of the EP. However, we keep A_0 here for two reasons. First, for a better comparison with the DP it is crucial to use unscaled diagonal elements. Second, the off-diagonal element A_0 turns out to be essential for the understanding of the sensitivity enhancement.

The reader can easily verify that $H_0|_{\mathrm{EP}}$ has just one linearly independent eigenvector

$$v_{\mathrm{EP}} = \begin{pmatrix} 1 \\ 0 \end{pmatrix}. \tag{4}$$

This is in contrast to $H_0|_{\mathrm{DP}}$ where two linearly independent eigenvectors can be constructed. The off-diagonal matrix element A_0 in Eq. (3) describes the backscattering to the direction of v_{EP}. There is no backscattering in the direction orthogonal to v_{EP}.

The signal to be detected is considered as a perturbation of the sensor and given by a general 2×2 Hamiltonian

$$H_1 = \begin{pmatrix} E_1 & A_1 \\ B_1 & E_1+\Delta E_1 \end{pmatrix}. \tag{5}$$

Here, E_1, ΔE_1, A_1, and B_1 are complex numbers. The full system is therefore described by the non-Hermitian matrix

$$H = H_0 + \varepsilon H_1, \tag{6}$$

with the formal perturbation parameter ε to be set to unity in the end. For comparison, H_1 is chosen to be the same both for the case of $H_0|_{\mathrm{DP}}$ and $H_0|_{\mathrm{EP}}$. Note, however, that in real systems such a comparison might be problematic, as the realization of the system at the DP and at the EP may require a different basis or even a different subspace of the full mode space.

A straightforward calculation shows that the eigenvalue splitting of H for the DP is of order ε:

$$\Delta E_{\mathrm{DP}} = \varepsilon\sqrt{(\Delta E_1)^2 + 4A_1B_1}. \tag{7}$$

The real part of ΔE_{DP} is the conventional frequency splitting. The imaginary part corresponds to a linewidth splitting. For the EP the splitting is of order $\sqrt{\varepsilon}$:

$$\Delta E_{\mathrm{EP}} = \sqrt{\varepsilon}\sqrt{\varepsilon(\Delta E_1)^2 + 4A_0B_1 + 4\varepsilon A_1B_1}, \tag{8}$$

provided that $B_1 \neq 0$. In that generic case, we can conclude that for sufficiently small perturbation the splitting at the EP is larger than at the DP. A counterexample with $B_1 = 0$ would be a perturbation induced by a rotation of the sensor as in the case of an optical gyroscope [39].

If both the sensor and the perturbation fulfill reciprocity, we can set $\Delta E_1 = 0$ as it is proven in Appendix A. Equations (7) and (8) then simplify to

$$\Delta E_{\mathrm{DP}} = 2\varepsilon\sqrt{A_1B_1} \tag{9}$$

and

$$\Delta E_{\mathrm{EP}} = 2\sqrt{\varepsilon}\sqrt{A_0B_1 + \varepsilon A_1B_1}. \tag{10}$$

This brings us to

$$\Delta E_{\mathrm{EP}} = \frac{\Delta E_{\mathrm{DP}}}{\sqrt{\varepsilon}}\sqrt{\varepsilon + \frac{A_0}{A_1}}, \tag{11}$$

and in lowest order with the formal perturbation parameter ε set to unity

$$\Delta E_{\mathrm{EP}} = \Delta E_{\mathrm{DP}}\sqrt{\frac{A_0}{A_1}}. \tag{12}$$

The simplified result in Eq. (12) holds for sufficient weak perturbations, in particular $|A_0| \gg |A_1|$ is required. This condition means that the intrinsic backscattering of the unperturbed system into the direction of v_{EP} is much larger than the backscattering into the same direction induced by the perturbation. Then, Eq. (12) tells us that the (complex) frequency splitting at the EP is much larger than the one at the DP even though in both cases the perturbation H_1 is exactly the same. For the absolute value of the frequency splitting we get

$$|\Delta E_{\mathrm{EP}}| = |\Delta E_{\mathrm{DP}}|\sqrt{\frac{|A_0|}{|A_1|}}. \tag{13}$$

The enhancement factor $|\Delta E_{\mathrm{EP}}|/|\Delta E_{\mathrm{DP}}|$ therefore does not depend on the phases of the matrix elements A_0, A_1, and B_1.

B. Passive and active systems

The eigenvalues $E_\pm$ of a 2×2 non-Hermitian Hamiltonian describing a passive system have to have a nonpositive imaginary part $\mathrm{Im}\, E_\pm \leqslant 0$ to avoid an increase of the eigensolutions $\psi_\pm e^{-iE_\pm t}$ in time. We call this the weak condition. A stronger condition is the requirement that the total intensity (probability)

$$I(t) = \psi(t)^\dagger\psi(t) \tag{14}$$

of any superposition

$$\psi(t) = a_+\psi_+ e^{-iE_+t} + a_-\psi_- e^{-iE_-t}, \tag{15}$$

with $a_\pm \in \mathbb{C}$, cannot increase at any point in time. These two conditions are different due to the nonorthogonality of the eigenvectors $\psi_+^\dagger\psi_- \neq 0$. To see this, we plug Eq. (15) into Eq. (14), use the normalization $\psi_\pm^\dagger\psi_\pm = 1$, and get

$$I(t) = |a_+|^2 e^{2\,\mathrm{Im}\,E_+t} + |a_-|^2 e^{2\,\mathrm{Im}\,E_-t} + 2\,\mathrm{Re}[a_+^* a_-\psi_+^\dagger\psi_- e^{i\mathrm{Re}(E_+-E_-)t}]e^{\mathrm{Im}(E_++E_-)t}. \tag{16}$$

The last term vanishes for orthogonal eigenvectors. In this special case, the weak and the strong conditions are identical. Note that the weak condition is related to a nonincreasing intensity averaged over the period $2\pi/|\mathrm{Re}(E_+ - E_-)|$ (ignoring the damping term).

It is in general not clear whether the strong condition is justified. Imagine a passive system where the leakiness comes from wave propagation to an environment, like an optical microcavity. In such a case, it is in principle possible that the intensity inside the system temporarily increases due to the interference of the two superimposed eigenstates provided that at the same time this increase is compensated in the environment. Here, only the averaged intensity is nonincreasing, satisfying the weak condition. For the optical microcavity that we study later in this paper we can prove in the two-mode approximation that the strong condition is indeed fulfilled. Also, for spatially closed systems where the openness comes from absorption inside the material, we expect the strong condition to be valid.

For a Hamiltonian of a reciprocal system in a suitable basis

$$H = \begin{pmatrix} E & A \\ B & E \end{pmatrix}, \tag{17}$$

the strong condition implies

$$2|\mathrm{Im}\,E| \geqslant |A - B^*|. \tag{18}$$

The original derivation of this inequality in Ref. [40] is rather lengthy. For the convenience of the reader, we attached in Appendix B a shorter and more transparent derivation.

In the following, we demonstrate that the strong condition for passive systems leading to the inequality (18) has an important consequence on the experimental observability of the real frequency splitting $\Delta E = |\mathrm{Re}\,E_+ - \mathrm{Re}\,E_-|$. To do so, we introduce the frequency-splitting quality

$$Q_{\mathrm{sp}} = \frac{\Delta E}{-\mathrm{Im}\,E_+ - \mathrm{Im}\,E_-}. \tag{19}$$

$Q_{\mathrm{sp}} > \frac{2}{3}$ should be satisfied to resolve the frequency splitting in a simple manner (note the slightly different definition of the mode-splitting quality in [41]). With the Hamiltonian (17) follows $\Delta E = 2|\mathrm{Re}\sqrt{AB}|$ and $\mathrm{Im}\,E_+ + \mathrm{Im}\,E_- = 2\,\mathrm{Im}\,E$. Putting this into Eq. (19) and using inequality (18) we find

$$Q_{\mathrm{sp}} = \frac{|\mathrm{Re}\sqrt{AB}|}{|\mathrm{Im}\,E|} \leqslant \frac{2|\mathrm{Re}\sqrt{AB}|}{|A - B^*|}. \tag{20}$$

With $|\mathrm{Re}\sqrt{AB}| \leqslant \sqrt{|A||B|}$ we finally get

$$Q_{\mathrm{sp}} \leqslant \frac{2\sqrt{|A||B|}}{|A - B^*|}. \tag{21}$$

In the situation of a slightly perturbed EP, we either have $|B| \ll |A|$ or $|A| \ll |B|$. In both cases, the frequency-splitting quality is well below unity according to the inequality (21). We conclude that in passive systems which fulfill the strong condition it is experimentally difficult to measure the frequency splitting by standard means.

For active systems, such as the ones studied in [25–27], the inequality (18) is not relevant. Therefore, introducing gain into the systems allows to overcome this experimental difficulty.

III. SINGLE WHISPERING-GALLERY MICROCAVITY

A. Two-state model with fixed azimuthal mode number

In this section we explain the two-state model for coupling of clockwise (CW) and counterclockwise (CCW) propagating waves in perturbed WG microcavities with fixed azimuthal mode number. This model was previously introduced to describe microcavity sensors for label-free, single-particle detection [25]. Examples of sensors based on WG modes are made of microdisks [42–44], microspheres [45,46], and microtoroids [6]. A target particle approaching the boundary of the microcavity evanescently couples to the CW and CCW propagating modes. It induces a backscattering between these modes resulting in frequency shifts and splitting of WG mode pairs. A measurement of the frequency splitting is more robust against fluctuations of the temperature and noise from the probe laser as compared to a measurement of a frequency shift [6,47].

We specify the sensor to be a WG microcavity which has been brought to an EP by two localized perturbations. Examples are a microtoroid with two nanofiber tips placed in the evanescent field of the modes [18] and a microdisk with two particles placed along the outer rim of the disk in the evanescent field of the modes [48]. In Ref. [48], an effective Hamiltonian has been introduced that describes a WG cavity with N local perturbations within a two-state approximation and slowly varying envelope approximation in the time domain [38]. With the azimuthal mode number $m \in \mathbb{N}$, radial mode number $l \in \mathbb{N}$ and the frequency $\Omega^{(0)} \in \mathbb{C}$ ($\mathrm{Im}\,\Omega^{(0)} \leqslant 0$ for a passive cavity) of the unperturbed WG modes the total effective Hamiltonian in the traveling-wave basis (CCW, CW) is given by the 2×2 non-Hermitian matrix

$$H^{(N)} = \begin{pmatrix} \Omega^{(N)} & A^{(N)} \\ B^{(N)} & \Omega^{(N)} \end{pmatrix} \tag{22}$$

with

$$\Omega^{(N)} = \Omega^{(0)} + \sum_{j=1}^{N}(V_j + U_j), \tag{23}$$

$$A^{(N)} = \sum_{j=1}^{N}(V_j - U_j)e^{-i2m\beta_j}, \tag{24}$$

$$B^{(N)} = \sum_{j=1}^{N}(V_j - U_j)e^{i2m\beta_j}. \tag{25}$$

The complex numbers $2V_j$ and $2U_j$ are frequency shifts for positive- and negative-parity modes introduced by local perturbation j alone ($\mathrm{Im}\, V_j \leqslant 0$ and $\mathrm{Im}\, U_j \leqslant 0$ for passive perturbations). For the microdisk geometry, these quantities can be calculated for the single localized perturbation either fully numerically, using, e.g., the boundary element method (BEM) [49], the finite-difference time-domain method [50], the finite-difference frequency-domain method [51], or approximately using the Green's function approach for point scatterers [52] ($U_j = 0$). It has been demonstrated that the two-state model (22)–(25) works very well for a disk with a few (but not too many) external scatterers [48].

The diagonal element $\Omega^{(N)} \in \mathbb{C}$ describes the frequency of the CCW and CW components in the absence of backscattering. The backscattering of CW and CCW propagating waves is described by the off-diagonal elements $A^{(N)}, B^{(N)} \in \mathbb{C}$. If the perturbed microcavity does not exhibit a mirror-reflection symmetry, then the backscattering is asymmetric with $|A^{(N)}| \neq |B^{(N)}|$. In such a case, the eigenvectors of $H^{(N)}$ show a kind of chirality which denotes here an imbalance of CCW and CW components. As a consequence, the optical modes are not standing waves but partially traveling waves [48,53,54], a fact that has been confirmed in a recent experiment [55]. Interestingly, the traveling-wave modes copropagate mainly in the same direction. Moreover, the optical mode pair is nonorthogonal [48,53,54]. The special case of fully asymmetric backscattering (e.g., $B^{(N)} = 0$ and $A^{(N)} \neq 0$) leads to an EP with collinear and fully chiral modes [48].

Note that the perturbed microcavity described by the Hamiltonian (22) in the traveling-wave basis does fulfill reciprocity, which is reflected by the fact that the diagonal matrix elements are equal. Moreover, a short calculation shows that the Hamiltonian (22)–(25) satisfies the inequality (18) for the case of passive cavity and passive perturbations, where the imaginary parts of $\Omega^{(0)}$, V_j, and U_j are nonpositive.

It is of importance to understand that the two-state model in Eqs. (22)–(25) based on a fixed azimuthal mode number m (and related coupled-mode models such as in [26,27]) in general differs from the two-state model near a DP/EP in Eqs. (2) and (3). The latter model is always a valid local description of a DP/EP of order two. The two-state model in this section may cover a different two-dimensional subspace of the full mode space and additionally requires that a single angular mode number $\pm|m|$ is sufficient to describe the system.

B. Microcavity sensor at an EP

In Ref. [25], the theory was restricted to the case of a microcavity sensor consisting of a WG microcavity with in total three local perturbations. The first two local perturbations implement the EP and the third one is disturbing it. In the two-state model with fixed angular mode number m, the microcavity sensor together with the target particle are described by Eq. (6) with $H_0 = H^{(2)}$ from Eq. (22), and

$$H_1 = \begin{pmatrix} V+U & (V-U)e^{-i2m\beta} \\ (V-U)e^{i2m\beta} & V+U \end{pmatrix} \tag{26}$$

using the shorthand notation $V = V_3$, $U = U_3$, $\beta = \beta_3$. For comparison with the splitting at a DP, we consider the disk without the two local perturbations which implement the EP. In the same spirit as in Sec. II, we compute the complex frequency splitting for the DP

$$\Delta\Omega_{\mathrm{DP}} = 2(V - U) \tag{27}$$

and, subsequently, the complex frequency splitting for the EP

$$\Delta\Omega_{\mathrm{EP}} = \Delta\Omega_{\mathrm{DP}}\sqrt{1 + \frac{A^{(2)}e^{i2m\beta}}{V-U}}. \tag{28}$$

The intrinsic backscattering can here be interpreted as backscattering of CW and CCW propagating waves. If this backscattering is much larger than the backscattering at the target particle $|A^{(2)}| \gg |V - U|$, then

$$\Delta\Omega_{\mathrm{EP}} = \Delta\Omega_{\mathrm{DP}}\, e^{im\beta}\sqrt{\frac{A^{(2)}}{V-U}}. \tag{29}$$

The real and imaginary parts of the complex frequency splitting $\Delta\Omega_{\mathrm{EP}}$ depend on the azimuthal position of the target particle β. However, the absolute value of the splitting is independent of β. Experimentally, it is necessary to measure both the frequency splitting $\mathrm{Re}(\Delta\Omega)$ and the linewidth splitting $-2\,\mathrm{Im}(\Delta\Omega)$. This can be done as recent experiments show [6,56].

If a gain material is introduced in the disk but not in the scatterers, then this increases only $\mathrm{Im}\,\Omega^{(0)}$. Hence, the gain does not change the real frequency splitting but it reduces the individual linewidths and therefore increases the frequency-splitting quality.

IV. NUMERICAL RESULTS

A. The system

We introduce a variation of the system studied in Refs. [25,48]. Here, the EP is initialized by two small holes inside the disk (cf. Fig. 1) (see, e.g., [52,57]). The target particle

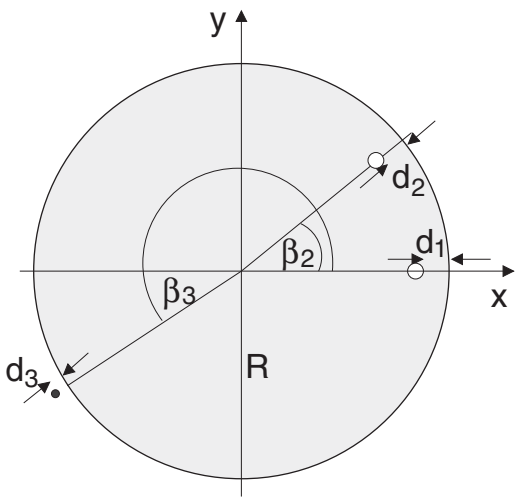

FIG. 1. Microdisk of refractive index n and radius R with three local scatterers [circles of refractive index n_j at distance d_j and at azimuthal position β_j ($\beta_1 = 0$)]. The two internal scatterers implement the exceptional point and the external scatterer is the target particle.

approaches the microdisk from the outside. In contrast to the geometry in Ref. [25], the two EP-generating scatterers do not conflict with the target particle. Surprisingly, as we will see in the following, this microcavity sensor cannot be described accurately with the theory developed in Ref. [25]. The more general theory presented in this paper is needed.

In total, we consider three local scatterers of radii r_j ($j = 1,2,3$) inside and outside of the microdisk of radius R. The precise shape of the target particle is not relevant in the regime of Rayleigh scattering where the wavelength λ is much larger than the size of the scatterers. The position of each local perturbation's center is $(x_3, y_3) = (R + r_3 + d_3)(\cos\beta_3, \sin\beta_3)$ and $(x_j, y_j) = (R - r_j - d_j)(\cos\beta_j, \sin\beta_j)$ for $j = 1,2$.

Maxwell's equations are solved in two dimensions within the effective index approximation with Sommerfeld outgoing-wave conditions at infinity. The optical modes are defined as the solutions with time dependence $e^{-i\omega t}$. We express the complex-valued frequency ω by the dimensionless frequency $\Omega = \frac{\omega}{c}R$ where c is the speed of light in vacuum. The real part is the conventional frequency whereas the imaginary part determines the linewidth (decay rate) $\gamma = -2\,\mathrm{Im}\,\Omega$ and the quality factor $Q = -\mathrm{Re}\,\Omega/[2\,\mathrm{Im}\,\Omega]$ of the given mode. The modes are determined numerically for transverse magnetic (TM) polarization using the BEM.

B. Sensor at the exceptional point

For the microcavity sensor we choose $n = 2 - i0.000\,45$ as refractive index of the disk including gain. For the two holes and the surrounding air we use a refractive index of unity. Moreover, $d_1/R = 0.18$, $d_2/R = 0.190\,161$, $r_1/R = 0.05$, $r_2/R = 0.069\,839$, $\beta_1 = 0$, and $\beta_2 = 0.523\,977$ in radian.

Figure 2 shows a pair of modes corresponding to unperturbed modes with azimuthal mode number $m = 15$ and the lowest radial mode number $l = 1$. This pair is close to an EP with $\Omega \approx 9.3510 - i0.0003$. The modes look very similar, which is consistent with the coalescence of the modes exactly at the EP. Moreover, no clear nodal line structure in azimuthal direction is visible, reflecting the chirality, i.e., the fact that the modes near such an EP are not standing waves but mainly (copropagating) traveling waves [48].

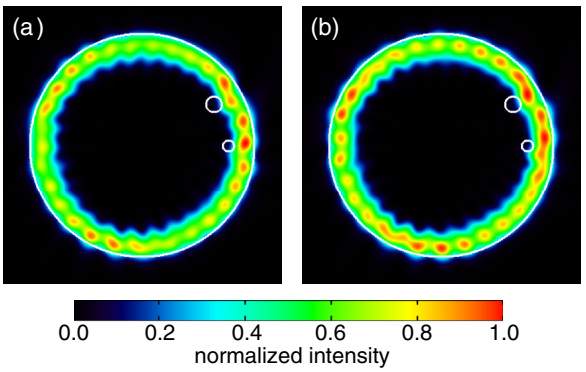

FIG. 2. Computed near-field intensity patterns of mode pair in the microcavity sensor (without target particle) close to an exceptional point. (a) Dimensionless frequency $\Omega_+ = 9.351\,021 - i0.000\,291$ and quality factor $Q_+ \approx 16\,000$. (b) $\Omega_- = 9.351\,033\,3 - i0.000\,304$ and $Q_- \approx 15\,400$.

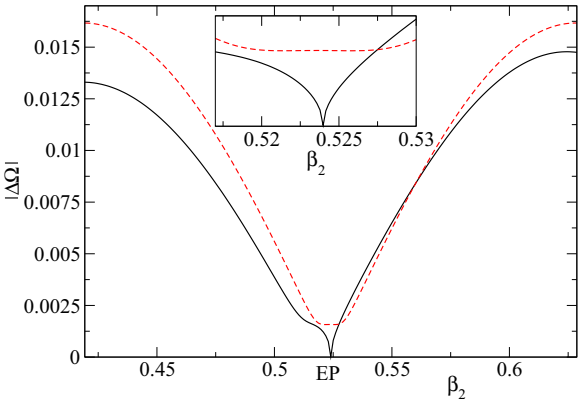

FIG. 3. Absolute value of the frequency splitting $|\Delta\Omega|$ as function of the azimuthal position β_2 of the second hole near the exceptional point (EP) ($\beta_2 = 0.523\,977$). The black solid (red dashed) curve is the result of the BEM [two-state model for fixed m in Eqs. (22)–(25)]. Inset: magnification around the EP.

Figure 3 confirms the square-root behavior of the frequency splitting near the EP by varying the azimuthal position β_2 of the second hole. Moreover, Fig. 3 shows a comparison to the two-state model with fixed azimuthal mode number m. The parameters V_j, U_j have been determined beforehand by BEM calculations for a disk with only a single hole. The β_2 dependence is then given analytically by Eqs. (22)–(25). While an overall agreement may be attested, it is obvious that the two-state model fails near the EP (see inset). This becomes even more obvious when we look at the off-diagonal elements of the Hamiltonian at the EP. We find for the absolute values of the off-diagonal elements 0.000 824 and 0.000 756, which is clearly in contradiction with the fact that the system is close to an EP. However, it has to be emphasized that this does not mean that the EP cannot locally be described by the two-state model in Eq. (3). As explained in Appendix C, we can extract the parameters of this more general two-state model from full BEM calculations and get for the absolute values of the off-diagonal elements 0.001 36 and 1.2×10^{-7} which indicates that the system is indeed very close to an EP.

We believe that the reason for the failure of the two-state model with fixed m is the fact that the internal perturbation by the holes more easily couples to angular components $|m'| \neq |m|$ if compared to the external perturbation by small scatterers (Ref. [48]). In fact, the holes can be a strong perturbation for angular momentum components $|m'| < |m|$ with radial mode number $l' > 1$ as the electric field reaches deeper into the microdisk.

C. Sensor with target particle

For the target particle with azimuthal position $\beta = \beta_3$, we fix in the following $d_3/R = 0.02, r_3/R = 0.005$, and $n_3 = 1.5$. The mode pair in the microcavity sensor with target particle at $\beta = 2$ is shown in Fig. 4. A careful comparison to Fig. 2 reveals a slightly more pronounced nodal line structure. This is because the target particle drives the system slightly away from the EP and thereby introduces a standing-wave component into the mode structure.

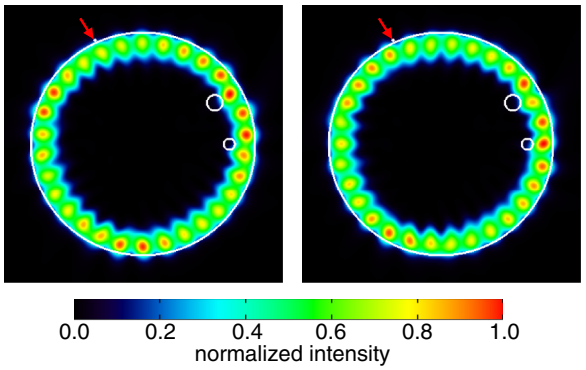

FIG. 4. Near-field intensity patterns of mode pair with the target particle at $\beta = 2$, marked by the arrow. (a) Dimensionless frequency $\Omega_+ = 9.350\,880\,8 - i0.000\,422$ and quality factor $Q_+ \approx 11\,100$. (b) $\Omega_- = 9.351\,134\,3 - 0.000\,186$ and $Q_- \approx 25\,200$.

Figure 5 shows the absolute value of the frequency splitting as function of the position of the target particle. For convenience, the splitting is normalized by the conventional splitting $|\Delta\Omega_{\mathrm{DP}}|$ occurring at a DP, which is the disk without holes. The full numerics (black curve) shows that the splitting is enhanced by an impressive factor of about 7. This clearly indicates the enhanced sensitivity of a sensor at an EP compared to a conventional one at a DP.

The dashed line in Fig. 5 is the result of Eq. (29). The parameters V and U are determined from BEM calculations for the disk with target particle but without holes. The parameter $|A^{(2)}| = 0.000\,824$ is determined as discussed in the previous section. The fact that $|B^{(2)}| = 0.000\,756 \neq 0$ is ignored here, which is actually not justified as $|A^{(2)}| \approx |B^{(2)}|$. Along with this inconsistency, we observe that the agreement of the result from the two-state model with fixed m to the full numerical result is not satisfying. The enhancement of the sensitivity is clearly underestimated.

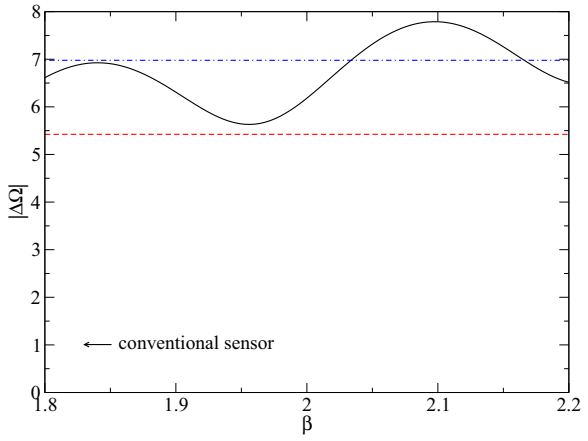

FIG. 5. Absolute value of the frequency splitting $|\Delta\Omega|$ normalized by the conventional splitting $|\Delta\Omega_{\mathrm{DP}}|$ vs target particle position β in radian. A more than sevenfold enhancement of the sensitivity compared to a conventional sensor is observed. The black solid curve is the full numerical solution. The red dashed line is the result of the two-state model with fixed azimuthal mode number in Eq. (29) and the blue dashed-dotted line is obtained from the general theory [see Eq. (13)]. In both cases, $B^{(2)}$ is set to zero.

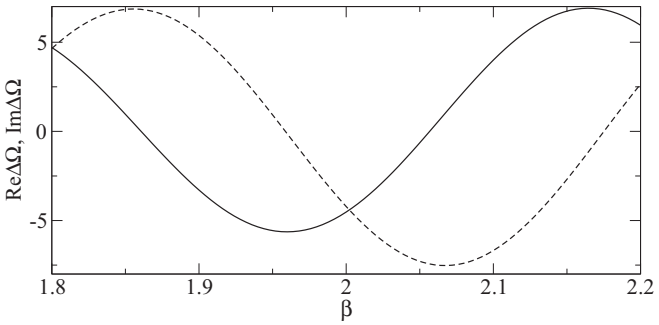

FIG. 6. Frequency splitting $\Delta\Omega$ from the full numerical calculations normalized by the conventional splitting $|\Delta\Omega_{\mathrm{DP}}|$ vs target particle position β in radian. The solid curve is the real part and the dashed curve is the imaginary part.

The dashed-dotted line in Fig. 5 is the result of the general theory [Eq. (13)], with $|A_0| = |A^{(2)}| = 0.001\,36$ as discussed in the previous section. Here, it is well justified to ignore $|B^{(2)}|$ as it is much smaller than $|A^{(2)}|$. The scattering strength $|A_1|$ of the target particle is estimated to be $|V - U|$ where we determine the parameters V and U from BEM calculations for the disk with target particle but without holes. This prediction of the enhancement of the sensitivity nicely agrees with the full numerical result. The oscillation of $|\Delta\Omega(\beta)|$ cannot be predicted as this requires to know the β dependence of $|A_1|$.

In our calculations we used a complex refractive index modeling optical gain to increase the frequency-splitting quality Q_{sp} as discussed in Sec. II B. In the context of microcavity sensors, optical gain has already experimentally used to reduce the linewidths [7,58]. However, here is still the problem that there are certain values of β at which the splitting $\mathrm{Re}(\Delta\Omega)$ vanishes (for example, at $\beta \approx 1.86$ as shown in Fig. 6). Near these values of β it is difficult to resolve the two peaks using a conventional Lorentzian curve fit, even though the linewidth splitting $|2\,\mathrm{Im}(\Delta\Omega)|$ is maximal. However, the harmonic inversion technique has proven to work reliably also in such extreme cases [59].

Considering that a single target particle induces a perturbation of order ε implies that $\tilde{N} \geqslant 2$ particles of the same type induce a perturbation of order $\tilde{N}\varepsilon$ when interference effects are ignored. From the considerations in Sec. II follow that the many-particle enhancement factor of the sensitivity is therefore expected to scale as $1/\sqrt{\tilde{N}\varepsilon}$. For the particular case studied in Fig. 5 with single-particle enhancement factor of about 7 we can therefore detect in the order of 49 particles before the enhancement factor becomes unity. When we consider the detection of the target particles one by one, then the individual increase of the splitting of particle $\tilde{N}$ (again ignoring interference effects) scales like $(\sqrt{\tilde{N}} - \sqrt{\tilde{N}-1})/\sqrt{\varepsilon} \approx 1/\sqrt{4\tilde{N}\varepsilon}$ when normalized to the result of the conventional sensor. For the situation in Fig. 5 that means that in the order of 12 particles can be detected one by one before the enhancement factor becomes unity.

V. DISCUSSION

In this paper we introduced a general theory of sensors for frequency- or energy-level-splitting detection based on

exceptional points. It was argued that the sensitivity of such a sensor is enhanced compared to a sensor based on a conventional degeneracy. For practical applications, the following conditions should be met: (i) both the frequency splitting and the linewidth splitting must be measured, (ii) the intrinsic backscattering at the exceptional point must be larger than backscattering induced by the perturbation, and (iii) the system must be active such that the two peaks can be resolved easily in experiments.

Numerical simulations on a microcavity sensor made of a microdisk with two holes demonstrated a sevenfold enhancement of the sensitivity. We showed that the previously introduced two-state model with fixed azimuthal mode number [25] does not describe this system accurately, whereas our general theory gives a good prediction of the enhancement factor. One message here is therefore that conclusions drawn exclusively from simple mode-coupling models such as in [26] may fail.

The general mechanism is not restricted to the geometry, size, wavelength, and refractive indices studied in this paper. Other microcavity geometries such as a deformed microdisk cavity at an EP [17] are possible. Further systems where our approach can be directly applied are, for instance, nanomechanical mass sensing using coupled cantilevers [13,60].

In this paper we considered second-order exceptional points, i.e., points in parameter space where only two eigenstates coalesce. At exceptional points of order $p > 2$ we expect an energy splitting of order $\varepsilon^{1/p}$ [10] which would give an even stronger enhancement of the sensitivity. Such higher-order exceptional points are, of course, more difficult to realize in experiments.

ACKNOWLEDGMENTS

Financial support by the DFG (Project No. WI1986/6-1) is acknowledged. I would like to thank S. Rotter for helpful discussions.

APPENDIX A: RECIPROCAL SYSTEMS

In this appendix, we show that for reciprocal systems one can chose $\Delta E_1 = 0$ in the matrix (5). We assume that both the unperturbed system and the perturbation fulfill reciprocity. In such a situation there is a common orthonormal basis (which is invariant under time reversal) in which the non-Hermitian Hamiltonians H_j are complex-symmetric matrices [31,61]. Note that in open systems the concepts of time-reversal symmetry and reciprocity are different [61,62]. We write

$$H_j = \begin{pmatrix} E_{1,j} & V_j \\ V_j & E_{1,j} \end{pmatrix}, \tag{A1}$$

where $E_{1,j}, V_j \in \mathbb{C}$ with $j = 1,2$. Using the unitary matrix

$$M^\dagger = \begin{pmatrix} \frac{1}{\sqrt{2}} & -\frac{i}{\sqrt{2}} \\ \frac{1}{\sqrt{2}} & \frac{i}{\sqrt{2}} \end{pmatrix} \tag{A2}$$

we transform H_j to

$$\tilde{H}_j = M^\dagger H_j M = \begin{pmatrix} E_j & A_j \\ B_j & E_j \end{pmatrix}, \tag{A3}$$

with

$$E_j = \frac{E_{1,j} + E_{2,j}}{2}, \tag{A4}$$

$$A_j = \frac{E_{1,j} - E_{2,j}}{2} - iV_j, \tag{A5}$$

$$B_j = \frac{E_{1,j} - E_{2,j}}{2} + iV_j. \tag{A6}$$

Note that in this basis the diagonal elements of each matrix $\tilde{H}_j$ are equal due to the assumed reciprocity.

In order to describe a twofold degeneracy, the elements of $\tilde{H}_0$ are either $A_0 = B_0 = 0$ [DP, see Eq. (2)] or $A_0 \neq 0$, $B_0 = 0$ [EP, see Eq. (3)] or $A_0 = 0$, $B_0 \neq 0$ (EP). The latter two cases are equivalent as a simple exchange of basis states proves. We therefore can restrict ourselves to the case with $B_0 = 0$.

APPENDIX B: PASSIVE SYSTEMS

We derive the inequality (18) for passive systems where the total intensity does not increase at any time. Using the Schrödinger-type equation (1) and the total intensity (probability) in Eq. (14), it is easy to show that

$$\frac{d}{dt} I = \psi^\dagger D \psi \tag{B1}$$

with the intensity-decay matrix

$$D = i(H^\dagger - H) = \begin{pmatrix} 2\,\mathrm{Im}\,E & i(B^* - A) \\ i(A^* - B) & 2\,\mathrm{Im}\,E \end{pmatrix}. \tag{B2}$$

The real eigenvalues of this Hermitian matrix are

$$d_\pm = 2\,\mathrm{Im}\,E \pm |A - B^*|. \tag{B3}$$

The condition $dI/dt \leqslant 0$ for all t implies that D is negative semidefinite. That means $d_\pm \leqslant 0$ which requires $\mathrm{Im}\,E \leqslant 0$ and, finally, inequality (18).

APPENDIX C: EXTRACTION OF MATRIX ELEMENTS NEAR AN EP

In this section, we show how to extract the parameters Ω, $|A|$, and $|B|$ of an effective Hamiltonian of the form

$$H = \begin{pmatrix} \Omega & A \\ B & \Omega \end{pmatrix} \tag{C1}$$

with eigenvalues and (not normalized) right eigenvectors

$$\Omega_\pm = \Omega \pm \sqrt{AB}, \tag{C2}$$

$$\psi_\pm = \begin{pmatrix} \sqrt{A} \\ \pm\sqrt{B} \end{pmatrix} \tag{C3}$$

near an EP from numerical mode calculations. Equation (C2) implies that we can compute from the numerical determined frequencies of the mode $\Omega_\pm^{\mathrm{num}}$ the parameter Ω and the product AB via

$$\Omega = \frac{\Omega_+^{\mathrm{num}} + \Omega_-^{\mathrm{num}}}{2}, \tag{C4}$$

$$AB = \frac{(\Omega_+^{\mathrm{num}} - \Omega_-^{\mathrm{num}})^2}{4}. \tag{C5}$$

We define the ratio $b = |B|/|A|$ with $b \ll 1$ near the EP. The normalized overlap between the two eigenvectors (C3) is

$$S = \frac{|A| - |B|}{|A| + |B|} = \frac{1-b}{1+b}. \tag{C6}$$

The normalized overlap can also be determined from the numerical calculation of the mode pair $\psi_\pm(x,y)$ via

$$S^{\text{num}} = \frac{\int dx\, dy\ \psi_+^* \psi_-}{\sqrt{\int dx\, dy\ \psi_+^* \psi_+}\sqrt{\int dx\, dy\ \psi_-^* \psi_-}}. \tag{C7}$$

From this we conclude that for $b \ll 1$ follows $2b = 1 - S^{\text{num}}$ and finally

$$|A| = \frac{|\Omega_+^{\text{num}} - \Omega_-^{\text{num}}|}{\sqrt{2}\sqrt{1 - S^{\text{num}}}}, \tag{C8}$$

$$|B| = \frac{|\Omega_+^{\text{num}} - \Omega_-^{\text{num}}|}{2\sqrt{2}}\sqrt{1 - S^{\text{num}}}. \tag{C9}$$

Equations (C4), (C8), and (C9) give Ω, $|A|$, and $|B| \ll |A|$ from the numerically determined values of $\Omega_\pm^{\text{num}}$ and S^{num}.

[1] L. Rondin, J.-P. Tetienne, T. Hingant, J.-F. Roch, P. Maletinsky, and V. Jacques, Rep. Prog. Phys. **77**, 056503 (2014).
[2] E. Gil-Santos, D. Ramos, J. Martínez, M. Fernández-Regúlez, R. García, A. San Paulo, M. Calleja, and J. Tamayo, Nat. Nanotechnol. **5**, 641 (2010).
[3] Y. Liu, L. Zhang, J. A. R. Williams, and I. Bennio, IEEE Photonics Technol. Lett. **12**, 531 (2000).
[4] W. W. Chow, J. Gea-Banacloche, L. M. Pedrotti, V. E. Sanders, M. O. Schleich, and W. Scully, Rev. Mod. Phys. **57**, 61 (1985).
[5] S. Sunada and T. Harayama, Opt. Express **15**, 16245 (2007).
[6] J. Zhu, Ş. K. Özdemir, Y.-F. Xiao, L. Li, L. He, D.-R. Chen, and L. Yang, Nat. Photonics **4**, 46 (2010).
[7] L. He, S. K. Özdemir, J. Zhu, W. Kim, and L. Yang, Nat. Nanotechnol. **6**, 428 (2011).
[8] F. Vollmer and L. Yang, Nanophotonics **1**, 267 (2012).
[9] M. V. Berry and M. Wilkinson, Proc. R. Soc. London, Ser. A **392**, 15 (1984).
[10] T. Kato, *Perturbation Theory for Linear Operators* (Springer, New York, 1966).
[11] W. D. Heiss, Phys. Rev. E **61**, 929 (2000).
[12] M. V. Berry, Czech. J. Phys. **54**, 1039 (2004).
[13] W. D. Heiss, J. Phys. A: Math. Gen. **37**, 2455 (2004).
[14] C. Dembowski, H.-D. Gräf, H. L. Harney, A. Heine, W. D. Heiss, H. Rehfeld, and A. Richter, Phys. Rev. Lett. **86**, 787 (2001).
[15] C. Dembowski, B. Dietz, H.-D. Gräf, H. L. Harney, A. Heine, W. D. Heiss, and A. Richter, Phys. Rev. E **69**, 056216 (2004).
[16] B. Dietz, T. Friedrich, J. Metz, M. Miski-Oglu, A. Richter, F. Schäfer, and C. A. Stafford, Phys. Rev. E **75**, 027201 (2007).
[17] S.-B. Lee, J. Yang, S. Moon, S.-Y. Lee, J.-B. Shim, S. W. Kim, J.-H. Lee, and K. An, Phys. Rev. Lett. **103**, 134101 (2009).
[18] J. Zhu, Ş. K. Özdemir, L. He, and L. Yang, Opt. Express **18**, 23535 (2010).
[19] Y. Choi, S. Kang, S. Lim, W. Kim, J.-R. Kim, J.-H. Lee, and K. An, Phys. Rev. Lett. **104**, 153601 (2010).
[20] M. Brandstetter, M. Liertzer, C. Deutsch, P. Klang, J. Schöberl, H. E. Türeci, G. Strasser, K. Unterrainer, and S. Rotter, Nat. Commun. **5**, 4034 (2014).
[21] H. Cartarius, J. Main, and G. Wunner, Phys. Rev. Lett. **99**, 173003 (2007).
[22] B. Alfassi, O. Peleg, N. Moiseyev, and M. Segev, Phys. Rev. Lett. **106**, 073901 (2011).
[23] H. Schomerus and J. Wiersig, Phys. Rev. A **90**, 053819 (2014).
[24] A. P. Seyranian, O. N. Kirillov, and A. A. Mailybaev, J. Phys. A: Math. Gen. **38**, 1723 (2005).
[25] J. Wiersig, Phys. Rev. Lett. **112**, 203901 (2014).
[26] A. Hassan, H. Hodaei, W. Hayenga, M. Khajavikhan, and D. Christodoulides, *Advanced Photonics 2015*, OSA Technical Digest (online) (Optical Society of America, Washington, DC, 2015), paper SeT4C.3, doi:10.1364/SENSORS.2015.SeT4C.3.
[27] S. Zhang, Z. Yong, Y. Zhang, and S. He, arXiv:1511.08802.
[28] T. Song, W. S. Lee, and K.-H. Ahn, Sci. Rep. **5**, 11470 (2015).
[29] N. Zhang, S. Liu, K. Wang, G. Z., L. Meng, N. Yi, S. Xiao, and Q. H. Song, Sci. Rep. **5**, 11912 (2015).
[30] I. Rotter, J. Phys. A: Math. Theor. **42**, 153001 (2009).
[31] H.-J. Stöckmann, E. Persson, Y.-H. Kim, M. Barth, U. Kuhl, and I. Rotter, Phys. Rev. E **65**, 066211 (2002).
[32] W. P. Reinhardt, Annu. Rev. Phys. Chem. **33**, 223 (1982).
[33] C. Keller, M. K. Oberthaler, R. Abfalterer, S. Bernet, J. Schmiedmayer, and A. Zeilinger, Phys. Rev. Lett. **79**, 3327 (1997).
[34] M. V. Berry and D. H. J. O'Dell, J. Phys. A: Math. Gen. **31**, 2093 (1998).
[35] S. Reitzenstein, S. Münch, P. Franeck, A. Löffler, S. Höfling, L. Worschech, A. Forchel, I. V. Ponomarev, and T. L. Reinecke, Phys. Rev. B **82**, 121306(R) (2010).
[36] G. E. Mitchell, A. Richter, and H. A. Weidenmüller, Rev. Mod. Phys. **82**, 2845 (2010).
[37] G. L. Celardo and L. Kaplan, Phys. Rev. B **79**, 155108 (2009).
[38] A. E. Siegman, *Lasers* (University Science Books, Sausalito, CA, 1986).
[39] R. Sarma, L. Ge, J. Wiersig, and H. Cao, Phys. Rev. Lett. **114**, 053903 (2015).
[40] B. Schlederer, Diploma thesis, Vienna University of Technology, 2013.
[41] Ş. K. Özdemir, J. Zhu, L. He, and L. Yang, Phys. Rev. A **83**, 033817 (2011).
[42] L. Chantada, N. I. Nikolaev, A. L. Ivanov, P. Borri, and W. Langbein, J. Opt. Soc. Am. B **25**, 1312 (2008).
[43] Q. H. Song and Y. L. Kim, J. Lightwave Technol. **28**, 2818 (2010).
[44] L. Deych, M. Ostroswski, and Y. Yi, Opt. Lett. **36**, 3154 (2011).
[45] F. Vollmer, S. Arnold, and D. Keng, Proc. Natl. Acad. Sci. USA **105**, 20701 (2008).
[46] J. T. Rubin and L. Deych, Phys. Rev. A **81**, 053827 (2010).
[47] L. Shao, X.-F. Jiang, X.-C. Yu, B.-B. Li, W. R. Clements, F. Vollmer, W. Wang, Y.-F. Xiao, and Q. Gong, Adv. Mater. **25**, 5616 (2013).
[48] J. Wiersig, Phys. Rev. A **84**, 063828 (2011).
[49] J. Wiersig, J. Opt. A **5**, 53 (2003).

[50] A. Taflove and S. C. Hagness, *Computational Electrodynamics the Finite-Difference Time-Domain Method* (Artech House, London, 2000).
[51] J. Shainline, S. Elston, Z. Liu, G. Fernandes, R. Zia, and J. Xu, Opt. Express **17**, 23323 (2009).
[52] C. P. Dettmann, G. V. Morozov, M. Sieber, and H. Waalkens, Phys. Rev. A **80**, 063813 (2009).
[53] J. Wiersig, S. W. Kim, and M. Hentschel, Phys. Rev. A **78**, 053809 (2008).
[54] J. Wiersig, A. Eberspächer, J.-B. Shim, J.-W. Ryu, S. Shinohara, M. Hentschel, and H. Schomerus, Phys. Rev. A **84**, 023845 (2011).
[55] M. Kim, K. Kwon, J. Shim, Y. Jung, and K. Yu, Opt. Lett. **39**, 2423 (2014).
[56] A. Mazzei, S. Götzinger, L. de S. Menezes, G. Zumofen, O. Benson, and V. Sandoghdar, Phys. Rev. Lett. **99**, 173603 (2007).
[57] S. Preu, S. I. Schmid, F. Sedlmeir, J. Evers, and H. G. L. Schwefel, Opt. Express **21**, 16370 (2013).
[58] L. He, S. K. Özdemir, J. Zhu, and L. Yang, Phys. Rev. A **82**, 053810 (2010).
[59] U. Kuhl, R. Höhmann, J. Main, and H.-J. Stöckmann, Phys. Rev. Lett. **100**, 254101 (2008).
[60] M. Spletzer, A. Raman, A. Q. Wu, and X. Xu, Appl. Phys. Lett. **88**, 254102 (2006).
[61] G. Dillon and G. Passatore, Nucl. Phys. A **114**, 623 (1968).
[62] R. Carminati, J. J. Sáenz, J.-J. Greffet, and M. Nieto-Vesperinas, Phys. Rev. A **62**, 012712 (2000).